



EARTH SCIENCES

Anthropogenic emission is the main contributor to the rise of atmospheric methane during 1993–2017

Zhen Zhang (张臻) ^{1,*}, Benjamin Poulter², Sara Knox³, Ann Stavert⁴, Gavin McNicol⁵, Etienne Fluet-Chouinard⁶, Aryeh Feinberg⁷, Yuanhong Zhao (赵园红)⁸, Philippe Bousquet⁹, Josep G. Canadell⁴, Anita Ganesan¹⁰, Gustaf Hugelius¹¹, George Hurtt¹, Robert B. Jackson^{6,12}, Prabir K. Patra¹³, Marielle Saunois⁹, Lena Höglund-Isaksson¹⁴, Chunlin Huang (黄春林)¹⁵, Abhishek Chatterjee^{16,17} and Xin Li (李新) ¹⁸

ABSTRACT

Atmospheric methane (CH₄) concentrations have shown a puzzling resumption in growth since 2007 following a period of stabilization from 2000 to 2006. Multiple hypotheses have been proposed to explain the temporal variations in CH₄ growth, and attribute the rise of atmospheric CH₄ either to increases in emissions from fossil fuel activities, agriculture and natural wetlands, or to a decrease in the atmospheric chemical sink. Here, we use a comprehensive ensemble of CH₄ source estimates and isotopic $\delta^{13}\text{C}$ -CH₄ source signature data to show that the resumption of CH₄ growth is most likely due to increased anthropogenic emissions. Our emission scenarios that have the fewest biases with respect to isotopic composition suggest that the agriculture, landfill and waste sectors were responsible for $53 \pm 13\%$ of the renewed growth over the period 2007–2017 compared to 2000–2006; industrial fossil fuel sources explained an additional $34 \pm 24\%$, and wetland sources contributed the least at $13 \pm 9\%$. The hypothesis that a large increase in emissions from natural wetlands drove the decrease in atmospheric $\delta^{13}\text{C}$ -CH₄ values cannot be reconciled with current process-based wetland CH₄ models. This finding suggests the need for increased wetland measurements to better understand the contemporary and future role of wetlands in the rise of atmospheric methane and climate feedback. Our findings highlight the predominant role of anthropogenic activities in driving the growth of atmospheric CH₄ concentrations.

Keywords: greenhouse gas, carbon cycle, climate mitigation, wetland, methane isotope

INTRODUCTION

Stabilizing atmospheric methane (CH₄) emissions from anthropogenic activities is a critical component of climate change mitigation [1]. The atmospheric CH₄ concentration has increased ~ 2.5 -fold from 731 ppb (parts per billion) in 1750 (pre-industrial reference year [2]) to 1890 ppb in 2020 [3]. Meanwhile, over the past century, atmospheric $\delta^{13}\text{C}$ -CH₄ values increased from $\sim -49.0\%$ in 1912 to -47.2% in 2007 due to increasing emissions of isotopically ¹³C-enriched (i.e. isotopically heavy) fossil fuels [4]. Despite the importance of under-

standing the temporal changes in atmospheric CH₄, the drivers of changes in the growth rate of atmospheric CH₄ over recent decades remain poorly understood [5]. The increase in atmospheric CH₄ slowed in the early 1990s and was followed by a so-called stabilization period during 2000–2006 [6]. Since 2007, global atmospheric CH₄ concentrations have begun to rise again, accompanied by a decline in $\delta^{13}\text{C}$ -CH₄ values from -47.2% in 2007 to -47.4% in 2017 [3]. The cause of this change has been studied recently using atmospheric inversion models [7–10], atmospheric box models [11–15] and

¹Department of Geographical Sciences, University of Maryland, College Park, MD 20742, USA; ²Biospheric Sciences Laboratory, NASA Goddard Space Flight Center, Greenbelt, MD 20771, USA; ³Department of Geography, University of British Columbia, Vancouver V6T 1Z2, Canada; ⁴Global Carbon Project, CSIRO Oceans and Atmosphere, Canberra, ACT 2601, Australia;

⁵Department of Earth and Environmental Sciences, University of Illinois Chicago, Chicago, IL 60607, USA; ⁶Department of Earth System Science, Stanford University, Stanford, CA 94305, USA; ⁷Institute for Data, Systems and Society, Massachusetts Institute of Technology, Cambridge, MA 02139, USA;

(Continued on next page)

*Corresponding author. E-mail: yuisheng@gmail.com

Received 15 July 2021; Revised 3 November 2021;

Accepted 3 November 2021

(Continued from previous page)

⁸College of Oceanic and Atmospheric Sciences, Ocean University of China, Qingdao 266000, China; ⁹Laboratoire des Sciences du Climat et de l'Environnement, LSCE-IPSL (CEA-CNRS-UVSQ), Université Paris-Saclay, Gif-sur-Yvette 91191, France; ¹⁰School of Geographical Sciences, University of Bristol, Bristol BS8 1RL, UK; ¹¹Department of Physical Geography and Bolin Centre for Climate Research, Stockholm University, Stockholm SE-106 91, Sweden; ¹²Woods Institute for the Environment and Precourt Institute for Energy, Stanford University, Stanford, CA 94305, USA; ¹³Research Institute for Global Change, JAMSTEC, Yokohama 236-0001, Japan; ¹⁴International Institute for Applied Systems Analysis (IIASA), Laxenburg A-2361, Austria; ¹⁵Northwest Institute of Eco-Environment and Resources, Chinese Academy of Sciences, Lanzhou 730000, China; ¹⁶Global Modeling and Assimilation Office, NASA Goddard Space Flight Center, Greenbelt, MD 20771, USA; ¹⁷Universities Space Research Association, Columbia, MD 21046, USA and ¹⁸Institute of Tibetan Plateau Research, Chinese Academy of Sciences, Beijing 100101, China

emission inventories [16]. These studies have arrived at divergent and even conflicting conclusions [17], citing increasing emissions of CH₄ from fossil fuels, agriculture, wetlands and/or decreased hydroxyl radicals (OH) as main drivers due to different measurements, methodologies and time periods considered (see Materials and Methods). Such discrepancies highlight the need to reconcile our understanding of the drivers of growth in atmospheric CH₄ in order to design mitigation policies [18].

Sources of the global CH₄ budget are mainly determined by three broadly defined groups: (i) thermogenic sources from industrial fossil fuel (e.g. coal, oil and natural gas; IFF_{CH₄}) and geological sources (GEO_{CH₄}); (ii) biogenic sources from livestock, rice agriculture, landfills and waste (AGW_{CH₄}), and natural wetlands (WET_{CH₄}); and (iii) pyrogenic sources from wildfires and biomass burning (BB_{CH₄}). The primary sink for CH₄ is reactions with tropospheric OH, soil microbial uptake and a small contribution from tropospheric chlorine reactions, which affect the isotopic compositions. The shift of the trend in atmospheric δ¹³C-CH₄ values towards more ¹³C-depleted (i.e. isotopically light) compositions suggests a higher dominance of isotopically light biogenic emissions in the global CH₄ budget [11,19]. This hypothesis has been supported by recent process-based and inversion modeling, which points to either a systematic underestimation of AGW_{CH₄} [20] or a large increase in WET_{CH₄} [8,10,21,22]. In contrast, there are large differences in the rate of change across inventory-based estimates of industrial fossil fuel source activity IFF_{CH₄} [23,24], as well as substantial underestimates in some regions and overestimates in other regions [12,25,26]. Globally, studies suggest that BB_{CH₄} has been declining, with fire CH₄ emissions associated with an isotopically enriched signature, thus providing room in the isotopic budget for an increase in fossil fuel sources [13]. GEO_{CH₄}, which is often co-located with the fossil fuel industry, is suggested to be largely overestimated by recent studies [27,28], indicating a potentially larger role of IFF_{CH₄} in affecting the global CH₄ budget given its underestimated share of the total CH₄ source [12,29].

OH oxidation in the troposphere is the main CH₄ sink, and reactions with chlorine (Cl), stratospheric sinks and soil removal are small-magnitude sinks. Substantial difficulties remain in quantifying CH₄ sinks, especially the main chemical sink for CH₄, tropospheric OH [5]. OH plays a significant but ambiguous role in driving the observed atmospheric trend; it is difficult to estimate due to its complicated chemistry, i.e. non-linear chemical feedback and short lifetime [30,31]. For example, estimates of interannual variability (IAV) in global mean OH are

significantly higher in the empirical box-model estimates that use CO and methylchloroform (MCF) constraints [32] than estimates based on chemical transport models (Fig. S1). Although there are debates on the potential biases in the box-model-based OH due to ignorance of complex spatial heterogeneity in OH and transport [33,34], the uncertainties in OH trends and variability are likely large enough to explain any potential CH₄ growth scenarios [14,15,35]. In addition, the trends in OH exert isotopic leverage on atmospheric δ¹³C-CH₄ values via the kinetic fractionation effect, such that increasing OH increases the atmospheric δ¹³C-CH₄ value by OH reacting with more ¹²CH₄. Therefore, it is of interest to investigate hypotheses regarding CH₄ sources with atmospheric δ¹³C-CH₄ observations while assuming that these sources can reproduce the atmospheric records with varying OH.

A thorough investigation of these hypotheses in a clearly defined framework is essential to help resolve the unexplained change in the growth rate of atmospheric CH₄. Here, we use an isotopic mass balance approach to attribute drivers of the growth rate of atmospheric CH₄ using a large ensemble of scenarios to represent different combinations of emission hypotheses (denoted emission scenarios, see Materials and Methods) from a comprehensive set of updated bottom-up estimates representing anthropogenic emission inventories and spatially explicit signatures for major CH₄ sources. Each emission scenario is composed of a time series of sectoral CH₄ fluxes and their hemispheric emission-weighted δ¹³C-CH₄ values. A globally representative database and spatially resolved distributions of δ¹³C-CH₄ values for the major CH₄ sources [36–38] were used to evaluate the temporal and regional variability in observed δ¹³C-CH₄ values. Monte Carlo techniques were applied to explore the uncertainty in δ¹³C-CH₄ estimates with full consideration of the spatial heterogeneity in CH₄ sources and their δ¹³C-CH₄ signatures. Scenario-specific parameters for the time series of the CH₄ removal rate driven by OH variations and run-specific ¹³CH₄ fractionation factors were derived by inverting an atmospheric two-box model (see Methods and Supplementary Data). We then evaluated the emission scenarios against observed δ¹³C-CH₄ values for 1993–2017 by running the two-box model in the forward mode. To test the hypothesis of a large increase from wetland CH₄ emissions, the idealized wetland scenarios (i.e. without process-based constraint) were then calculated to reproduce the temporal pattern of δ¹³C-CH₄. The comparison against atmospheric isotopic observations allowed us to select the most likely set of emission scenarios, which are defined as the first percentile cut-off of the lowest mean squared difference (MSD) in simulated δ¹³C-CH₄ values.

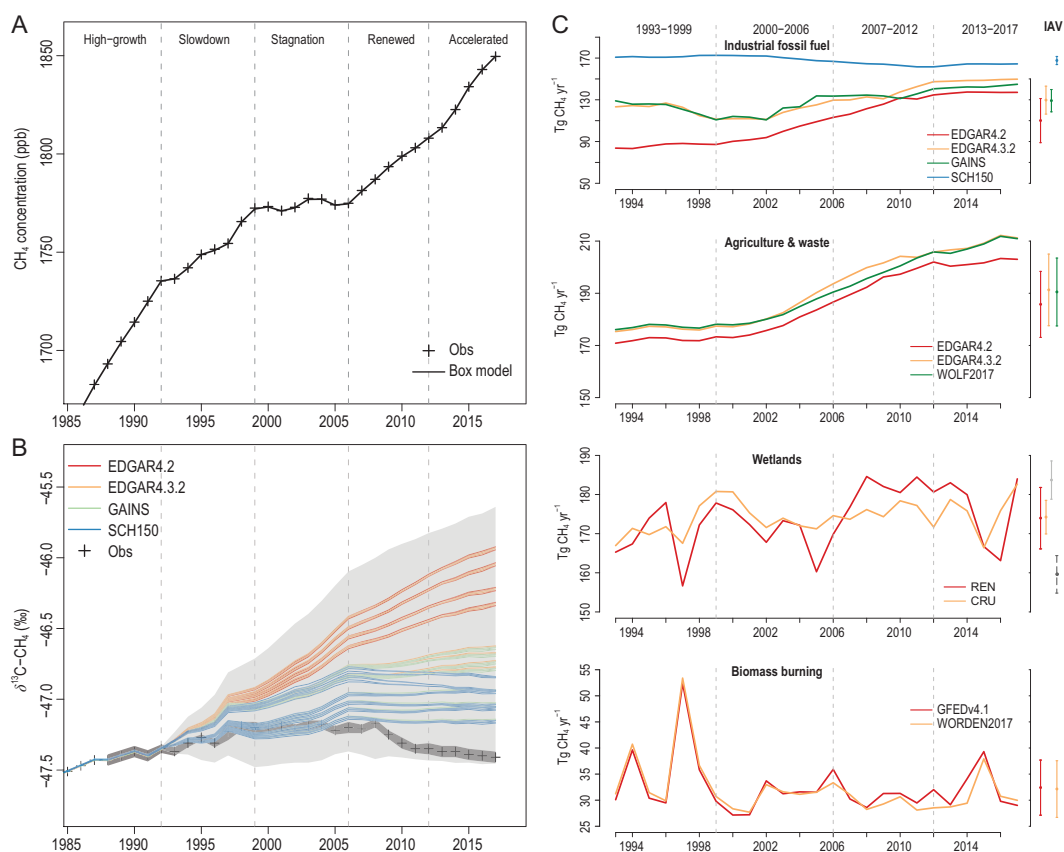


Figure 1. Simulated global atmospheric CH₄ concentration, $\delta^{13}\text{C-CH}_4$ values and bottom-up estimates of major CH₄ sources. (A) Simulated atmospheric CH₄ concentration (black solid line) from all emission scenarios exactly reproducing the observed CH₄ records (cross dots). The ensemble simulations of the box model were run in forward mode with prescribed $\delta^{13}\text{C-CH}_4$ variations from emission scenarios using OH time series derived from inverse mode (Fig. S1). (B) Simulated ensemble mean $\delta^{13}\text{C-CH}_4$ values (colored solid lines) for emission scenarios grouped by industrial fossil fuel inventories (EDGARv4.2, EDGARv4.3.2, GAINS and SCH150) in comparison to the observed global mean $\delta^{13}\text{C-CH}_4$ (cross). The uncertainty range of ensemble simulations ($n = 96\ 000$) and $1-\sigma$ uncertainty of the observations are shown as light gray areas and dark gray areas, respectively. (C) Time series of annual total emissions for major sources. The interannual variability ($1-\sigma$) in CH₄ for each individual bottom-up estimate is shown at the right of the plot. Note that for the wetland category, the dashed bars represent two independent estimates from a bottom-up ensemble of wetland models [40] for 2000–2012 (light gray) and WetCHARTs [41] (dark gray) for 2001–2015.

RESULTS AND DISCUSSION

Temporal variations in the atmospheric CH₄ concentration and its $\delta^{13}\text{C-CH}_4$ value

The ensemble simulations for the 96 emission scenarios ($4\ \text{IFF}_{\text{CH}_4} \times 3\ \text{AGW}_{\text{CH}_4} \times 2\ \text{WET}_{\text{CH}_4} \times 2\ \text{BB}_{\text{CH}_4} \times 2\ \text{GEO}_{\text{CH}_4}$) reproduced the observed atmospheric CH₄ concentration (Fig. 1A) using the corresponding optimized time series of OH derived from running the box model in inverse mode (Fig. S1). We accounted for the uncertainty in source signatures of $\delta^{13}\text{C-CH}_4$ by resampling 1000 sets of $\delta^{13}\text{C-CH}_4$ signature time series for each emission scenario ($n = 96 \times 1000$), which resulted in a wide range of modeled atmospheric $\delta^{13}\text{C-CH}_4$ values with some closely reproducing the observations. However, most emission scenarios

tended to generate more enriched $\delta^{13}\text{C-CH}_4$ trends for 1993–2017, suggesting that existing bottom-up inventories overestimate the increase in IFF_{CH_4} during the study period, especially during slowdown and stagnation periods (Fig. 1B). Furthermore, to balance the rise in CH₄ sources, the increases in OH levels also led to positive trends in atmospheric $\delta^{13}\text{C-CH}_4$ values during these two periods (Fig. S1). Note that the large increase in coal-related emissions since 2003 has increased the $\delta^{13}\text{C-CH}_4$ values of the sources, which contribute to the divergence between the model and observations. The timing of this divergence is consistent with a rapid increase in methane emissions from China (mainly coal emissions) as reported by the inventories [23] and inversions [39]. For most of the emission scenarios, the estimated temporal variations in

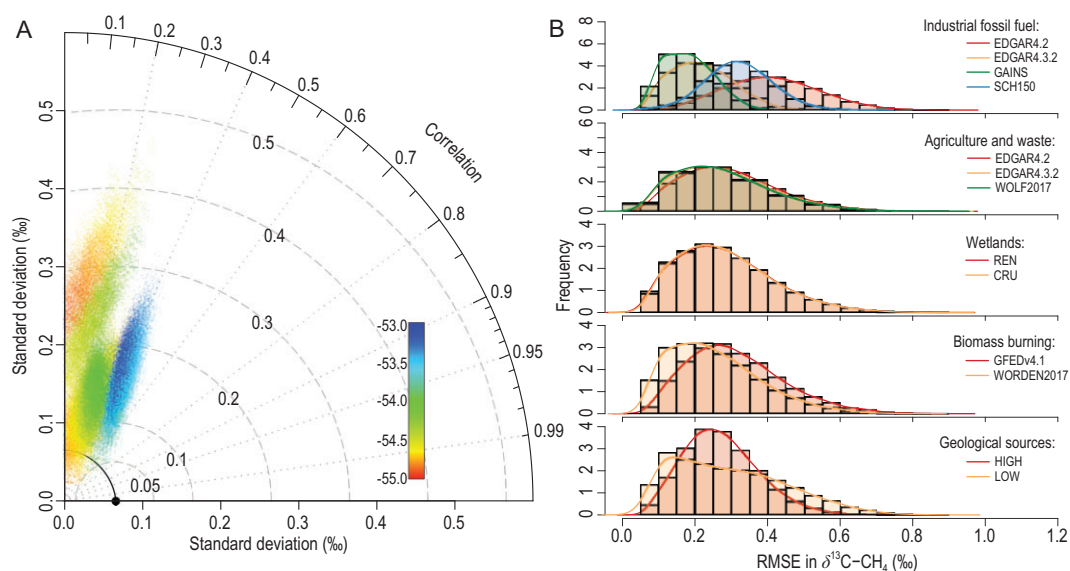


Figure 2. Performance of emission scenarios in simulating atmospheric $\delta^{13}\text{C-CH}_4$. (A) Taylor diagram illustrating the similarity between individual time series from the 96 000 simulations of different emission scenarios (colored dots) to the observed atmospheric $\delta^{13}\text{C-CH}_4$ for 1993–2017. The black solid dot refers to the observed global average $\delta^{13}\text{C-CH}_4$ for 1993–2017. Each dot symbol indicates the correlation value (angle), the standard deviation (SD, radial distance to the origin point) and the root mean square error (RMSE, distance to the black solid dot), with different colors representing the mean global average $\delta^{13}\text{C-CH}_4$ value of the source. (B) Histograms of RMSE between simulated $\delta^{13}\text{C-CH}_4$ values and observations grouped by bottom-up estimates with different colors for major CH_4 source categories. The solid lines represent the fitted density distribution after spline smoothing.

OH for 1993–2017 fall within the $1\text{-}\sigma$ range of the Bayesian inversion from Ref. [14] and are in good agreement with Ref. [35] for the post-2000 period. The EDGARv4.2-based emission scenarios have the largest mismatch with the inversion-based OH anomaly (relative to a global mean concentration of 1e^6 molecules (molec)/ cm^3), confirming the known higher bias in EDGARv4.2 than in other inventories (Fig. S2).

The time series of CH_4 sources for 1993–2017 (Fig. 1C) suggests that decadal-scale variations in atmospheric CH_4 are dominated by anthropogenic emissions from both agricultural and fossil fuel activities. However, there is high uncertainty across IFF $_{\text{CH}_4}$ inventories, with a sizable (>40 Tg CH_4 yr^{-1}) difference in magnitude and a large difference in temporal trends between inventories (i.e. EDGARv4.2, EDGARv4.3.2 and GAINS) and an atmospheric-observation-constrained approach (i.e. SCH150, which hypothesizes that IFF $_{\text{CH}_4}$ is underestimated but does not increase over time). The temporal variation in AGW $_{\text{CH}_4}$ exhibits a lower discrepancy than IFF $_{\text{CH}_4}$ in the inventories, whereas WET $_{\text{CH}_4}$ and BB $_{\text{CH}_4}$ are more constrained. The IAV and magnitude of our estimates for WET $_{\text{CH}_4}$, calculated using the process-based model LPJ-wsl, are comparable to the ensemble mean of multiple wetland models [40] and a global wetland CH_4 emission model ensemble for use in atmospheric chemi-

cal transport models (WetCHARTs) [41]. The wetland CH_4 estimates derived from driving the wetland model with a ground-measurement-based meteorological dataset from the Climate Research Unit (CRU) yield a small increase (<1 Tg CH_4 yr^{-1}), whereas the same model with climate reanalysis (REN) has an ~ 7.3 Tg CH_4 step increase from tropical wetlands between 2000–2006 and 2007–2017 [22].

Evaluations of proposed CH_4 hypotheses using emission scenarios

Figure 2A shows the distribution of residual bias in the individual box model simulations in terms of how they reproduce the observed $\delta^{13}\text{C-CH}_4$ values. In the Taylor diagram [42] the global average $\delta^{13}\text{C-CH}_4$ values of the sources before fractionation by chemical sinks range from -53‰ to -55‰ over 1993–2017, and a correlation coefficient lower than 0.6 is obtained for all of the simulations for 1993–2017. The low agreement suggests that the biases in the inventories and the wetland models contribute to the discrepancies in reproducing the $\delta^{13}\text{C-CH}_4$, which is likely due to the overestimated increase in inventories, especially the coal emission that has a relatively heavy isotopic signature, as found by previous atmospheric inversion studies [16]. In addition, some of the simulations can reproduce similar IAV in atmospheric $\delta^{13}\text{C-CH}_4$ values with root mean

square errors (RMSEs) from 0.05‰ to 0.5‰, but ~85% of simulations tend to produce higher IAV than observed. Although the global average $\delta^{13}\text{C-CH}_4$ value was regarded as observational ‘truth’, this reference has an uncertainty of 0.04‰, attributed to variability in measurements across all the stations and uncertainty from scale conversions between networks [43].

The density distributions of RMSEs grouped by different bottom-up CH_4 estimates show the divergent performance of emission scenarios in reproducing observed atmospheric $\delta^{13}\text{C-CH}_4$ values (Fig. 2B). Among the four IFF_{CH₄} inventories, 80% of the simulations using EDGARv4.2 generated more positive trends of $\delta^{13}\text{C-CH}_4$ values than the other three inventories, with no EDGARv4.2-based runs located in the most likely set of emission scenarios (Fig. S3). This result corroborates previous studies that also suggest that EDGARv4.2 tends to overestimate fossil fuel growth [44]. The more recent EDGARv4.3.2 has been improved, with 95% of the simulations located within the RMSE range from 0.1‰ to 0.3‰, mainly due to improved emission factors and revised statistics of CH_4 sectors [23]. SCH150 produces lower agreement than EDGARv4.3.2 partly due to the low IAV of SCH150, as SCH150 focuses on the long-term trends in IFF_{CH₄}. The GAINS inventories generated better performance: 78% of the simulations in the first percentile of MSD are based on GAINS IFF_{CH₄}. Note that this does not rule out the IFF_{CH₄} scenarios that have flat or insignificant trends (e.g. SCH150), as ^{13}C -enriched BB_{CH₄} estimates in this study show declining trends over recent years, which would allow for compensation by increasing emissions from IFF_{CH₄} to meet the decreasing atmospheric $\delta^{13}\text{C-CH}_4$ values. Generally, IFF_{CH₄} has a more pronounced impact in determining the past trends in $\delta^{13}\text{C-CH}_4$ changes than the other major CH_4 sources.

The contribution of combined agriculture, landfills and waste included in AGW_{CH₄}, which together represent 50%–62% of all anthropogenic sources, again reveals a higher bias of EDGARv4.2-based simulations compared to the other two inventories (Fig. 2B). Agricultural emissions dominate AGW_{CH₄}, with an average contribution of 77.5% to the total AGW_{CH₄} over the study period. The lower MSD scores using EDGARv4.3.2 and WOLF2017 emission scenarios show improved reconciliation of estimates for the AGW_{CH₄} source relative to the isotopic budget. This result supports the hypothesis that the global livestock estimates based on the 2006 IPCC Tier 1 guidelines underestimate livestock CH_4 emissions at the national or state level [45], which is potentially attributable to outdated

information used to develop the emission factors. However, there is no clear signal to distinguish whether EDGARv4.3.2 or WOLF2017 has a lower a priori bias, suggesting the need for further regional and global assessments by spatially explicit 4-D atmospheric models.

Our calculations suggest that, in contrast to anthropogenic sources, wetland CH_4 emissions play a limited role in reproducing the decadal trend in atmospheric $\delta^{13}\text{C-CH}_4$ (Figs 1 and 2B). Both REN and CRU demonstrate that wetland CH_4 emissions appear to have contributed little to the renewed growth in atmospheric CH_4 . However, wetland emissions help explain the IAV in the atmospheric CH_4 growth rate via its pulsed responses to climate dynamics, such as the El Niño–Southern Oscillation [46]. The latitudinal gradient of the growth rate for CH_4 sources (Fig. S4) suggests that WET_{CH₄} in the tropics has an important impact on the IAV of the CH_4 growth rate, albeit the current limited understanding of WET_{CH₄} is due to a significant deficiency in WET_{CH₄} measurements in the tropics, especially for Africa [21].

The density distribution of RMSE grouped by BB_{CH₄} and GEO_{CH₄} (Fig. 2B) suggests that the recent hypotheses regarding a larger decrease [13] in BB_{CH₄} and overestimated contemporary GEO_{CH₄} [27,28] have a good agreement with the isotopic budget. The lower RMSE of Worden (2017)-based scenarios supports the hypothesis of a decreasing trend in BB_{CH₄} during the post-2007 period, as suggested by inversion modeling based on satellite measurements of carbon monoxide [47]. The low GEO_{CH₄} scenarios, which assume a geological source of 15 Tg $\text{CH}_4 \text{ yr}^{-1}$ with upward-revised IFF_{CH₄} (see Methods and Supplementary Data), yield lower RMSEs than the conventional high-GEO_{CH₄} scenarios in which GEO_{CH₄} was set to 52 Tg $\text{CH}_4 \text{ yr}^{-1}$. These findings support the hypothesis that the current bottom-up estimates of anthropogenic fossil fuel CH_4 emissions are underestimated and that geological emissions are overestimated.

Changes in the trends of $\delta^{13}\text{C-CH}_4$ source signatures

A change in source signature (Fig. 3A) suggests varying global-emission-weighted average sources driven by the change in spatiotemporal distribution of CH_4 source estimates for the four major CH_4 categories. When considering spatial heterogeneity in the source signature, the globally representative $\delta^{13}\text{C-CH}_4$ values tend to suggest a larger variation than previous assumptions that use globally uniform values [7,13]. The IFF_{CH₄}

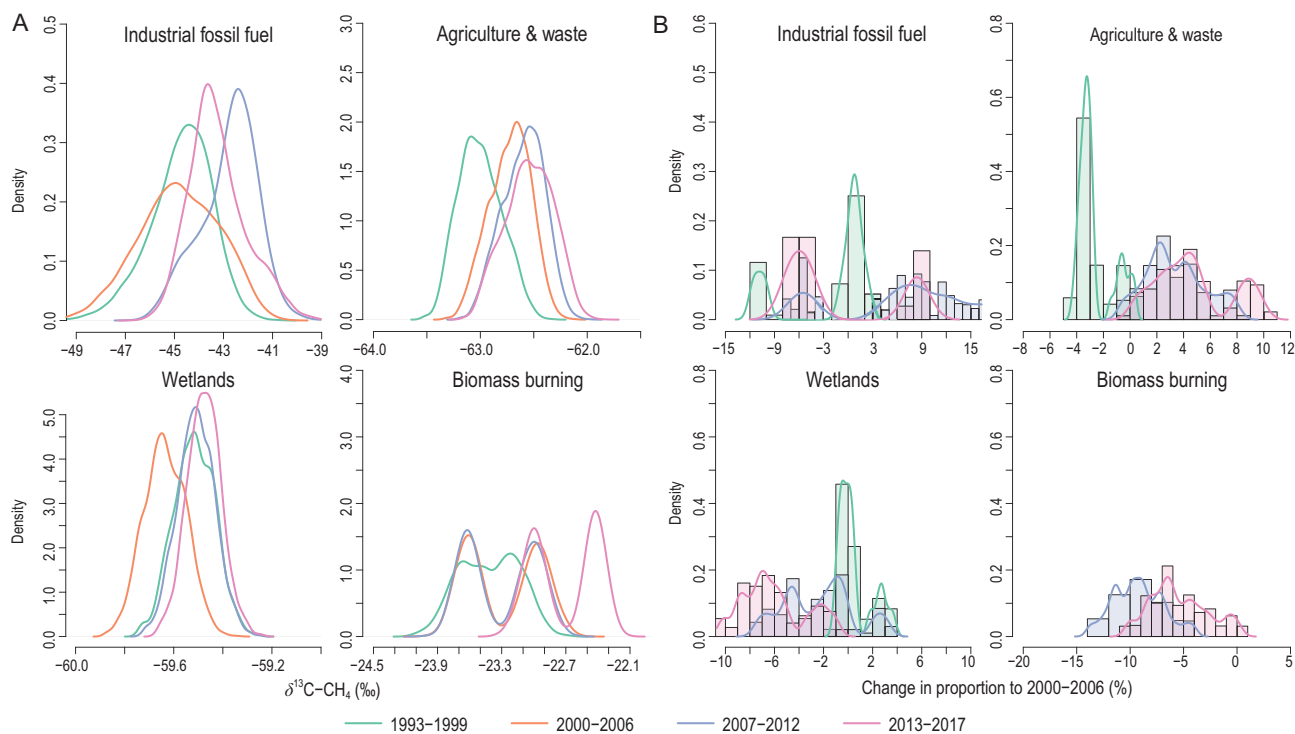


Figure 3. Changes in $\delta^{13}\text{C}-\text{CH}_4$ values and in contribution of $^{13}\text{CH}_4$ mass to the annual total of $^{13}\text{CH}_4$ mass for major source categories during 1993–2017. (A) Density function of the mean emission-weighted $\delta^{13}\text{C}-\text{CH}_4$ value of the sources for four time periods from Monte Carlo accounting ($n = 96\,000$): decreased atmospheric growth during 1993–1999, relative stabilization during 2000–2006, renewed growth during 2007–2012 and accelerated growth during 2013–2017. While the emission-weighted $\delta^{13}\text{C}-\text{CH}_4$ signatures may change over time, it is the combination of these signatures with their respective emission amounts that determines the atmospheric isotopic trend. (B) Density distribution of changes in the contribution of $^{13}\text{CH}_4$ mass from major CH_4 source categories to annual global $^{13}\text{CH}_4$ mass. The contribution of $^{13}\text{CH}_4$ mass is calculated as the average percentage change of the ratio of average annual total $^{13}\text{CH}_4$ mass in the source during 1993–1999, 2007–2012 and 2013–2017 relative to the CH_4 plateau period 2000–2006.

signature varies between time periods from a median of -44.9‰ during 2000–2006 to a median of -42.7‰ during 2013–2017, suggesting high variability in the $\delta^{13}\text{C}-\text{CH}_4$ values of anthropogenic CH_4 sources. The AGW_{CH_4} signature slightly increased from a median value of -62.5‰ to -62.3‰ from 2000–2006 to post-2007. Note that the effect of the decreasing trend of atmospheric $\delta^{13}\text{C}-\text{CO}_2$ values on the C_3-C_4 diet composition of domestic ruminants in recent decades was not taken into account in this study; consideration of this factor would yield a slight decrease in the AGW_{CH_4} signature [48]. Wetland $\delta^{13}\text{C}-\text{CH}_4$ values increased slightly from -59.7‰ to -59.5‰ from the stabilization period to the renewed-growth period, mainly attributable to increased tropical wetland CH_4 emissions since 2007. Tropical wetlands tend to have a more enriched signature (mean -56.7‰) than northern high-latitude peatland-based wetlands (mean -67.8‰) (Fig. S5), as supported by a few site-level measurements [36,38,49]. The possible signature enrichment from wetlands is another line of evidence for a weak wetland CH_4 emission response [22,40], while there is no evidence of a signif-

icant change in wetland CH_4 from high latitudes in either model [16,44] or by direct atmospheric measurement [50], where the rise of WET_{CH_4} may possibly be counteracted by increased soil uptake [51]. However, it is difficult to distinguish CH_4 from wetlands and livestock, as the signatures of the two sectors are similar and the spatial distributions are possibly co-located [3], suggesting a critical need for more measurements to provide better constraints on $\delta^{13}\text{C}-\text{CH}_4$ values in the tropics.

The change in the $\delta^{13}\text{C}-\text{CH}_4$ contribution from individual sources does not necessarily imply the same trend in the global average signature. Theoretically, even if the tropical wetland signature becomes more positive, the increased proportion of wetland-contributed $^{13}\text{CH}_4$ mass to the total $^{13}\text{CH}_4$ mass can still result in a shift towards a more negative global signal, as the biogenic signature is considerably lighter than the global atmospheric $\delta^{13}\text{C}-\text{CH}_4$ value [36] ($\sim -53.6\text{‰}$) before fractionation. This is the case in some paleoclimate studies [52] where tropical wetlands and other natural sources (e.g. biomass burning) dominated the annual CH_4 budget. However, the role of human activities has

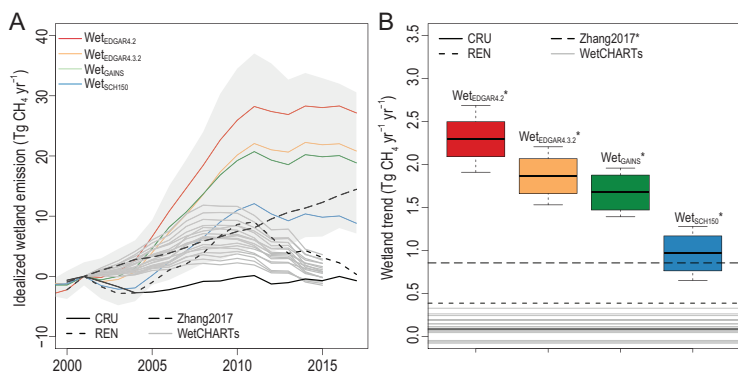


Figure 4. Idealized wetland emissions that reproduce the observations of atmospheric CH₄ and δ¹³C-CH₄ for 2000–2017. (A) Time series of anomalies of idealized WET_{CH4} with a 7-year moving window (colored lines: ensemble mean grouped by IFF_{CH4}) in comparison to the two emission scenarios (CRU and REN) applied in this study and the estimates from Ref. [53] (denoted Zhang2017) and WetCHARTs [41]. All estimates are anomalies relative to 2001. The min/max range of idealized wetland emissions is shown as the gray area. (B) Trend of wetland emissions for 2000–2017 computed using linear regression. Significant trends at the 95% confidence level are denoted with ‘*’.

become dominant in the annual CH₄ and isotope budgets since AD 1750, and the relative importance of wetlands has lessened. Figure 3B also shows the probability distribution of the relative contribution of ¹³CH₄ mass to the annual total ¹³CH₄ mass in the source, from 2000–2006 to the post-2007 period. IFF_{CH4} exhibits either an increased contribution of 5%–8% based on EDGARv4.2 or a decreased contribution of 6%–9% relative to 2000–2006 based on SCH150 or GAINS. In contrast to IFF_{CH4}, AGW_{CH4} shows a significantly increasing contribution to the isotope budget from 2000–2006 to the post-2007 period, with a positive trend of 5%–7% relative to 1993–1999. This pattern can be explained by the substantial increase in AGW_{CH4} production since the 21st century. The contribution of BB_{CH4} to the ¹³CH₄ mass was 20%–25% lower in 2007–2017 than in 1993–1999 and 2000–2006, mainly due to reduced biomass burning, as suggested by the inversion model based on satellite retrievals [13] and by inventories [47].

Idealized wetland emission scenarios that reproduce the decrease in atmospheric δ¹³C-CH₄ values

Beyond our wetland-model ensemble, we created scenarios to investigate the possible involvement of rising WET_{CH4} in the decrease of atmospheric δ¹³C-CH₄ values. To do so, we performed a sensitivity test by running the box model in inverse mode for each individual run to calculate idealized WET_{CH4} given the other sources, varying OH concentration, atmospheric CH₄ and δ¹³C-CH₄ observations, and the isotopic signatures of the sources, which thus

linearizes the problem. The results suggest that the magnitude of increase in idealized WET_{CH4} largely depends on the hypothesis of IFF sources, where greater wetland increases are required to compensate for the large increase in the IFF_{CH4} scenarios (Fig. 4A). Note that all the idealized WET_{CH4} scenarios are higher than the two WET_{CH4} scenarios in this study (i.e. CRU and REN) or WetCHARTs, a wetland CH₄ product that is based on satellite-derived surface water extent and precipitation reanalysis and an ensemble of ecosystem respiration estimates. One process-based WET_{CH4} that overlaps the increases in idealized wetland scenarios is the ensemble mean of LPJ-wsl simulations for a future projection under the climate scenario RCP8.5 [53] (denoted Zhang2017). RCP8.5 is considered the upper bound of wetland CH₄ feedback to rising temperature in LPJ-wsl because the strong and steady increase in temperature in RCP8.5 is higher than that determined from actual observations. Note that this scenario would occur only in combination with the hypothesis that IFF_{CH4} has had no significant trends in recent years.

The comparison of 2000–2017 trends in WET_{CH4} (Fig. 4B) suggests that to reproduce the magnitude of the observed decrease in atmospheric δ¹³C-CH₄ values, the required emission increase from natural wetlands would need to be much higher than the current estimates from process-based wetland models. The trend of CRU is consistent with the ensemble estimate of global wetland model simulations [5,40], while that of REN is at the higher end of the trends that consider the potential inundation increase due to enhanced tropical precipitation [22]. Note that the range of idealized increases in WET_{CH4} is in line with two recent inversion studies [8,10] based on GOSAT CH₄ measurements, which suggests a positive wetland trend of 2–3 Tg CH₄ yr⁻¹ yr⁻¹ for 2010–2018. However, to produce such a significant trend, the Q10 parameter (temperature sensitivity of CH₄ emissions) in the wetland models would need to be much higher than the range of 2–3 from LPJ-wsl and WetCHARTs or the measurement-based average of 2.57 from FLUXNET-CH₄ [54]. In addition, a recent multi-model ensemble inversion study [55] suggests that the observation-constrained wetland CH₄ feedback to rising temperature is lower than that of Zhang 2017. Despite this, there are considerable uncertainties in modeled WET_{CH4} due to scarcity of measurements for the tropics [40]. We conclude that the hypothesis that a large increase in natural wetlands drives the decrease in atmospheric δ¹³C-CH₄ values cannot be reconciled with process-based wetland CH₄ models.

Table 1. Statistics of global representative average $\delta^{13}\text{C}-\text{CH}_4$ values for the major CH_4 categories used in the Monte Carlo simulations for 1993–2017. The interannual variability (IAV), uncertainty propagated from bottom-up estimates, and the full uncertainty that considers both uncertainty from emissions and spatially resolved distribution of source signatures for different CH_4 categories are listed. See Table S2 for CH_4 sectors that are not shown here.

$\delta^{13}\text{C}-\text{CH}_4$ (‰)	Mean	IAV	Uncertainty	Full
			from emissions	uncertainty
Coal	−45.8	0.71	1.23	2.57
Oil & gas	−43.8	0.06	0.61	0.93
Livestock	−65.4	0.16	0.32	0.86
Wetlands	−59.6	0.10	0.15	0.20
Biomass burning ^a	−23.9	0.38	0.03	0.14

^aThe higher IAV of BB_{CH_4} than the uncertainty range is due to the spikes during some extreme El Niño years, which are one order of magnitude higher than that of most years.

Attributions of the CH_4 rise based on the most likely scenarios

Our Monte Carlo estimation (Table 1) suggests that the largest uncertainties in global representative source $\delta^{13}\text{C}-\text{CH}_4$ values are in industrial fossil fuel activities, providing clues for future studies. Our estimated global representative values for total CH_4 source signatures are within the uncertainty of recently compiled databases [12,36] but are lower than the value used in previous inverse studies (see Fig. S6 for references). Among the major CH_4 emis-

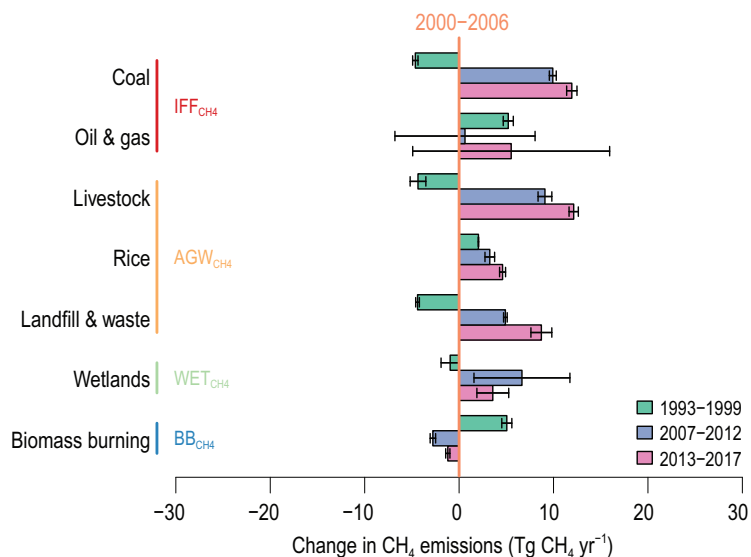


Figure 5. Changes in average total CH_4 emissions in the most likely scenarios. The changes in CH_4 emissions over the three periods are calculated relative to the average in the CH_4 plateau period 2000–2006 (vertical reference line in orange). The most likely scenarios are defined as the subset of emission scenarios ($n = 960$) in the first percentile lowest mean squared difference (MSD) (Fig. S6) in comparison to the full ensembles ($n = 96\,000$; Fig. S9). IFF_{CH_4} , AGW_{CH_4} , WET_{CH_4} and BB_{CH_4} represent the CH_4 sectors of industrial fossil fuels, agriculture and waste, wetlands, and biomass burning, respectively.

sion sectors, the global average emission-weighted $\delta^{13}\text{C}-\text{CH}_4$ signature for coal has the highest IAV, which is mainly due to the large deviation in country-level data in coal emissions [39] and the heterogeneous distribution of different coal ranks [56]. Note that the low-rank coals tend to produce isotopically lighter CH_4 [36] with a potentially biogenic origin [57], indicating that the proportion of consumption of different coal types may have a significant impact on atmospheric $\delta^{13}\text{C}-\text{CH}_4$ values.

We calculate the most likely scenarios based on the agreement of bottom-up estimates with isotopic observations (Fig. 5). The results suggest that the agricultural, landfill and waste sectors account for $53 \pm 13\%$ ($21.0 \pm 0.8 \text{ Tg CH}_4 \text{ yr}^{-1}$; $1-\sigma$) of renewed growth over the period of 2007–2017 compared to 2000–2006, with industrial fossil fuel sources and wetland sources contributing $34 \pm 24\%$ ($13.7 \pm 8.8 \text{ Tg CH}_4 \text{ yr}^{-1}$) and $13 \pm 9\%$ ($5.3 \pm 3.5 \text{ Tg CH}_4 \text{ yr}^{-1}$), respectively. The decreasing emissions from fossil fuel sectors in 1993–1999 compared to 2000–2006, combined with the increasing OH anomaly (Fig. S8), may have contributed to the CH_4 stabilization period (Fig. 5 and Fig. S7). The increases in methane emissions (mainly from the fossil fuel, agriculture and waste sectors) combined with a step increase from wetland CH_4 and small decreases in OH levels led to renewed growth in methane during 2007–2012. Moreover, the higher CH_4 emissions from mainly anthropogenic activities, i.e. coal, oil, gas, livestock, landfill and waste sectors, drove the accelerated increase in atmospheric CH_4 during 2013–2017. These sectoral emission increases are consistent with economic activity data (Table S2; Table S3) showing that, in the past decade, coal production has increased by 41.7% globally (International Energy Agency, <https://www.iea.org/topics/coal/statistics/>) and that the populations of major livestock species (e.g. swine, chickens and ruminant animals) have increased by 22.5% (FAO-STAT, <http://www.fao.org/faostat/>). Although coal production exhibited a temporary decline during 2014–2016 (Statistical Review of World Energy 2020, <https://www.bp.com/content/dam/bp/business-sites/en/global/corporate/pdfs/energy-economics/statistical-review/bp-stats-review-2020-full-report.pdf>), average coal emissions during 2013–2017 were higher than those during 2007–2012, indicating that coal mining emissions continued to grow, with a higher contribution to the increase in atmospheric CH_4 .

CONCLUSIONS

Our analysis shows that a comprehensive evaluation of hypotheses regarding the attribution of rising

atmospheric CH₄ based on a combination of bottom-up approaches and isotopic values can reconcile multiple lines of evidence into a robust global CH₄ budget. However, we acknowledge that there are some biases and uncertainties in the bottom-up estimates and that our exploration of possible emission scenarios does not cover all potential scenarios. This study clearly suggests that the proposed hypotheses are influenced by the choice of a priori estimates, indicating that the high-bias a priori estimates of trends applied in some earlier studies have led to equally biased conclusions regarding the attribution of atmospheric methane rise. Our results suggest that decreasing emissions from coal, oil and gas from 1993–1999 to 2000–2006, combined with the increasing OH anomaly, likely contributed to the methane stabilization period. Anthropogenic sources were the most likely major contributor to the renewed growth in CH₄ after 2006. Moreover, the good agreement of low present-day geological source estimates with observations supports the hypothesis that the IFF_{CH₄} in recent decades has been largely underestimated. However, our understanding of the role of livestock and wetlands, particularly in tropical regions, is more limited [58,59]. Aircraft measurements in these regions may help address the lack of data and improve our understanding of WET_{CH₄}. This study highlights the dominant role of anthropogenic emissions from fossil fuels, agriculture, landfills and waste in driving the recent rising trend in atmospheric CH₄. Our findings improve our understanding of the causes of changes in atmospheric CH₄ over the past 25 years, enabling the development of more targeted mitigation strategies and policies to stabilize and ultimately reduce key contributing emission sectors.

MATERIALS AND METHODS

Model descriptions

The model was developed from previous studies [15,60,61] and consists of two perfectly mixed boxes representing the troposphere in the northern and southern hemispheres. The changes in CH₄ concentration are calculated using the following equations:

$$\begin{aligned}
 {}^{12}\text{CH}_4^{\text{N}}(t + \Delta t) = & {}^{12}\text{CH}_4^{\text{N}}(t) \\
 & + \left(\sum_i {}^{12}S_i^{\text{N}}(t) + \sum_j k_j^{1212} \text{CH}_4^{\text{N}}(t) \right. \\
 & \left. - \frac{1}{2\tau_{\text{ex}}} {}^{12}\text{CH}_4^{\text{N}}(t) + \frac{1}{2\tau_{\text{ex}}} {}^{12}\text{CH}_4^{\text{S}}(t) \right) \Delta t, \quad (1)
 \end{aligned}$$

$$\begin{aligned}
 {}^{12}\text{CH}_4^{\text{S}}(t + \Delta t) = & {}^{12}\text{CH}_4^{\text{S}}(t) \\
 & + \left(\sum_i {}^{12}S_i^{\text{S}}(t) + \sum_j k_j^{1312} \text{CH}_4^{\text{S}}(t) \right. \\
 & \left. - \frac{1}{2\tau_{\text{ex}}} {}^{12}\text{CH}_4^{\text{S}}(t) + \frac{1}{2\tau_{\text{ex}}} {}^{12}\text{CH}_4^{\text{N}}(t) \right) \Delta t, \quad (2)
 \end{aligned}$$

where ¹²CH₄ is approximated by CH₄ and ¹²S_{*i*}^N(*t*) and ¹²S_{*i*}^S(*t*) represent the annual source strength of the source in the northern hemisphere and southern hemisphere, respectively. *k*¹² is the first-order removal rate coefficient for the sinks. The interhemispheric exchange time τ is set to a constant value of 1 yr given that the overall methane CH₄ concentration and OH anomalies are largely unaffected by the interhemispheric exchanges [15].

The $\delta^{13}\text{C}$ -CH₄ isotopic signatures of the different source categories *i* and the kinetic isotope effect (KIE) in the individual sink reactions *j* are used to calculate the sources (¹³S_{*i*}) and removal rate coefficients (¹³k_{*j*}) for $\delta^{13}\text{C}$ -CH₄ values.

These terms are then used to derive the mixing ratio changes in ¹³C-CH₄:

$$\begin{aligned}
 {}^{13}\text{CH}_4^{\text{N}}(t + \Delta t) = & {}^{13}\text{CH}_4^{\text{N}}(t) \\
 & + \left(\sum_i {}^{13}S_i^{\text{N}}(t) + \sum_j k_j^{1313} \text{CH}_4^{\text{N}}(t) \right. \\
 & \left. - \frac{1}{2\tau_{\text{ex}}} {}^{13}\text{CH}_4^{\text{N}}(t) + \frac{1}{2\tau_{\text{ex}}} {}^{13}\text{CH}_4^{\text{S}}(t) \right) \Delta t, \quad (3)
 \end{aligned}$$

$$\begin{aligned}
 {}^{13}\text{CH}_4^{\text{S}}(t + \Delta t) = & {}^{13}\text{CH}_4^{\text{S}}(t) \\
 & + \left(\sum_i {}^{13}S_i^{\text{S}}(t) + \sum_j k_j^{1313} \text{CH}_4^{\text{S}}(t) \right. \\
 & \left. - \frac{1}{2\tau_{\text{ex}}} {}^{13}\text{CH}_4^{\text{S}}(t) + \frac{1}{2\tau_{\text{ex}}} {}^{13}\text{CH}_4^{\text{N}}(t) \right) \Delta t. \quad (4)
 \end{aligned}$$

The mixing ratios of the individual isotopologues are converted to δ values as follows:

$$\delta_{\text{C}}^{13} = \left(\frac{{}^{13}\text{CH}_4 / {}^{12}\text{CH}_4}{{}^{13}\text{R}_{\text{std}}} - 1 \right), \quad (5)$$

where $^{13}R_{\text{std}} = 1.12372\%$ is the $^{13}\text{C}/^{12}\text{C}$ ratio of the international reference material Vienna Pee Dee Belemnite (VPDB).

The soil sink is considered to have a low IAV, as suggested by biogeochemical models [62,63], despite a recent study [64] based on a few site-level measurements suggesting a decline in the soil sink in temperate forests in recent decades. For soil CH_4 uptake, we use climatology from a process-based model [63] in the calculation of the hemispheric net CH_4 source (see equation 6 in Materials and Methods). The contributions of Cl sink and stratospheric loss to the removal of CH_4 in the troposphere are highly uncertain and not well constrained by direct observations, but have a strong kinetic isotope effect on $^{13}\text{CH}_4$. Given the large uncertainty in Cl and stratospheric sinks and the lack of available datasets, the magnitudes of these two sinks were not explicitly considered in the calculation of the hemispheric CH_4 budget. We assume that the annual methane removal rate is driven solely by OH variability, while other minor sinks are kept constant over the study period. Because sensitivity tests [65] suggest that the uncertain magnitude of Cl fields leads to a wide range of simulated $\delta^{13}\text{C}\text{-CH}_4$ values given its strong ‘isotope leverage’ effect [66] ($-60 \pm 1\%$) on total ε , the sink-weighted average fractionation factor ε is highly uncertain. The approach in this study is to estimate the total ε value for each box model run that optimizes the match between atmospheric observations and simulation at the onset of the study period. The optimized ε values were derived from running the box model in inverse mode by matching the observed global average [11]. This allows us to explore the uncertainty in ε based on bottom-up source aggregation and the uncertainty in $\delta^{13}\text{C}\text{-CH}_4$ values. Figure S6 shows that the estimated fractionation factors for the full ensemble and first percentile ensemble are broadly in agreement with previous studies [11–13,60,66–70]. The distribution of the mean methane lifetime (Fig. S9) over the study period is slightly lower than the estimated 9.1 ± 0.9 yr from Ref. [71] and is comparable in magnitude to that between atmospheric chemistry-transport models in the recent model intercomparison [31,32,72]. Here, we evaluate the global results from the box model, instead of hemispheric results, to minimize the potential influence of uncertainty in IAV from inter-hemispheric transport on box model performance, as suggested by a recent study [73]. See Supplementary Data for details about the model strategy.

CH₄ source estimates

To test all the proposed competing hypotheses, we carried out simulation experiments using box modeling for different emission scenarios based on a suite

of bottom-up datasets. We first list all the possible options for the CH_4 inventories by five CH_4 source categories (i.e. IFF_{CH_4} , AGW_{CH_4} , WET_{CH_4} , BB_{CH_4} and GEO_{CH_4}) and then generate emission scenarios with combinations of CH_4 inventories. The assignment of the inventory (i.e. EDGAR)-specific sectors into the main categories IFF_{CH_4} , AGW_{CH_4} and BB_{CH_4} follows the criteria from Supplementary Table S4 in Ref. [5]. Anthropogenic CH_4 emissions related to fossil fuels from exploitation, transportation and usage of coal, oil and natural gas are defined as IFF_{CH_4} . For methane sectors related to enteric fermentation and manure, landfills, waste and rice agriculture are defined as AGW_{CH_4} .

Spatially resolved $\delta^{13}\text{C}\text{-CH}_4$ and uncertainty estimation

Spatially resolved distributions of $\delta^{13}\text{C}\text{-CH}_4$ source signatures for the following major methane categories were applied in this study: coal, natural gas/oil, livestock, wetlands and biomass burning. For the other sources, including agricultural waste, rice, geological sources, termites, freshwater systems and wild animals, we use a globally averaged value (Table S4) from a global inventory database that collected isotopic source signatures based on literature values [36,66,68].

Emission scenarios

An emission scenario is a combination of the individual CH_4 source estimates listed in Table S1. Annual total net CH_4 sources can be expressed as follows:

$$S_{\text{tot}} = S_{\text{IFF}} + S_{\text{AGW}} + S_{\text{WET}} + S_{\text{BB}} + S_{\text{GEO}}, \\ + S_{\text{OTH}} - S_{\text{soil}}, \quad (6)$$

where S represents the individual CH_4 source from Table S1 and S_{soil} is a constant soil sink. The total number of emission scenarios is 96, calculated as $4 \text{ IFF}_{\text{CH}_4} \times 3 \text{ AGW}_{\text{CH}_4} \times 2 \text{ WET}_{\text{CH}_4} \times 2 \text{ BB}_{\text{CH}_4} \times 2 \text{ GEO}_{\text{CH}_4}$. For each emission scenario, we use Monte Carlo techniques to estimate the uncertainty in the source signature propagated from bottom-up estimates and the spatial variability of the source signature. A set of 1000 random maps of $\delta^{13}\text{C}\text{-CH}_4$ values for each major CH_4 source (Table 1) were generated based on the uncertainty maps in this study assuming a Gaussian distribution. For CH_4 sources that are not spatially resolved, 1000 samples of the global-representative signature values are calculated with mean and 1-standard deviation defined by observations from the compiled databases (Table S4). One thousand sets of emission-weighted hemispheric time series of $\delta^{13}\text{C}\text{-CH}_4$, which were

calculated with bottom-up estimates depending on emission scenarios, were used as inputs for the box model. For each emission scenario, the simulated time series of $\delta^{13}\text{C}-\text{CH}_4$ values covers the uncertainty range of spatial variability in the isotopic signatures of major CH_4 categories.

DATA AVAILABILITY

All data needed to evaluate the conclusions in this paper are present in the paper and/or the Supplementary Data. Additional ancillary data are available from the corresponding author upon request.

SUPPLEMENTARY DATA

Supplementary data are available at [NSR](#) online.

ACKNOWLEDGEMENTS

We thank A.J. Turner for sharing the basis of our box model, G. Janssens-Maenhout *et al.* for sharing the EDGAR inventories and O. Sherwood for sharing the database of $\delta^{13}\text{C}-\text{CH}_4$ signatures. We thank S. Schwietzke, N. Chandra and S. Strode for their constructive comments. J.G.C. and A.S. are grateful for the support of the Australian National Environmental Science Program-Earth Systems and Climate Change Hub. We thank the University of Colorado's Institute of Arctic and Alpine Research (INSTAAR) (<https://instaar.colorado.edu>) and National Oceanic and Atmospheric Administration (NOAA) Earth System Research Laboratory (ESRL) (<https://www.esrl.noaa.gov>) for sharing the atmospheric $\delta^{13}\text{C}-\text{CH}_4$ measurements.

FUNDING

We acknowledge support from the Strategic Priority Research Program of the Chinese Academy of Sciences (XDA19040504 and XDA19070204) and the Gordon and Betty Moore Foundation through grant GBMF5439 'Advancing Understanding of the Global Methane Cycle' supporting the Methane Budget released by the Global Carbon Project (globalcarbonproject.org). P.K.P. is partly supported by the Environment Research and Technology Development Fund (JPMEERF20182002) of the Environmental Restoration and Conservation Agency of Japan.

Conflict of interest statement. None declared.

REFERENCES

- Ocko IB, Sun T and Shindell D *et al.* Acting rapidly to deploy readily available methane mitigation measures by sector can immediately slow global warming. *Environ Res Lett* 2021; **16**: 054042.
- Meinshausen M, Vogel E and Nauels A *et al.* Historical greenhouse gas concentrations for climate modelling (CMIP6). *Geosci Model Dev* 2017; **10**: 2057–116.
- Nisbet EG, Manning MR and Dlugokencky EJ *et al.* Very strong atmospheric methane growth in the 4 years 2014–2017: implications for the Paris Agreement. *Glob Biogeochem Cycles* 2019; **33**: 318–42.
- Ferretti DF. Unexpected changes to the global methane budget over the past 2000 years. *Science* 2005; **309**: 1714–7.
- Saunois M, Stavert AR and Poulter B *et al.* The global methane budget 2000–2017. *Earth Syst Sci Data* 2020; **12**: 1561–623.
- Nisbet EG, Dlugokencky EJ and Bousquet P. Methane on the rise—again. *Science* 2014; **343**: 493–5.
- Thompson RL, Nisbet EG and Pisso I *et al.* Variability in atmospheric methane from fossil fuel and microbial sources over the last three decades. *Geophys Res Lett* 2018; **45**: 11499–508.
- Yin Y, Chevallier F and Ciais P *et al.* Accelerating methane growth rate from 2010 to 2017: leading contributions from the tropics and East Asia. *Atmos Chem Phys* 2021; **21**: 12631–47.
- He J, Naik V and Horowitz LW *et al.* Investigation of the global methane budget over 1980–2017 using GFDL-AM4.1. *Atmos Chem Phys* 2020; **20**: 805–27.
- Zhang Y, Jacob DJ and Lu X *et al.* Attribution of the accelerating increase in atmospheric methane during 2010–2018 by inverse analysis of GOSAT observations. *Atmos Chem Phys* 2021; **21**: 3643–66.
- Schaefer H, Fletcher SEM and Veidt C *et al.* A 21st-century shift from fossil-fuel to biogenic methane emissions indicated by $^{13}\text{C}_4$. *Science* 2016; **352**: 80–4.
- Schwietzke S, Sherwood OA and Bruhwiler LMP *et al.* Upward revision of global fossil fuel methane emissions based on isotope database. *Nature* 2016; **538**: 88–91.
- Worden JR, Bloom AA and Pandey S *et al.* Reduced biomass burning emissions reconcile conflicting estimates of the post-2006 atmospheric methane budget. *Nat Commun* 2017; **8**: 2227.
- Rigby M, Montzka SA and Prinn RG *et al.* Role of atmospheric oxidation in recent methane growth. *Proc Natl Acad Sci USA* 2017; **114**: 5373–7.
- Turner AJ, Frankenberg C and Wennberg PO *et al.* Ambiguity in the causes for decadal trends in atmospheric methane and hydroxyl. *Proc Natl Acad Sci USA* 2017; **114**: 5367–72.
- Saunois M, Bousquet P and Poulter B *et al.* Variability and quasi-decadal changes in the methane budget over the period 2000–2012. *Atmos Chem Phys* 2017; **17**: 11135–61.
- Turner AJ, Frankenberg C and Kort EA. Interpreting contemporary trends in atmospheric methane. *Proc Natl Acad Sci USA* 2019; **116**: 2805–13.
- Nisbet EG, Fisher RE and Lowry D *et al.* Methane mitigation: methods to reduce emissions, on the path to the Paris Agreement. *Rev Geophys* 2020; **58**: e2019RG000675.
- Nisbet EG, Dlugokencky EJ and Manning MR *et al.* Rising atmospheric methane: 2007–2014 growth and isotopic shift: rising methane 2007–2014. *Glob Biogeochem Cycles* 2016; **30**: 1356–70.
- Wolf J, Asrar GR and West TO. Revised methane emissions factors and spatially distributed annual carbon fluxes for global livestock. *Carbon Balance Manage* 2017; **12**: 16.
- Lunt MF, Palmer PI and Feng L *et al.* An increase in methane emissions from tropical Africa between 2010 and 2016 inferred from satellite data. *Atmos Chem Phys* 2019; **19**: 14721–40.
- Zhang Z, Zimmermann NE and Calle L *et al.* Enhanced response of global wetland methane emissions to the 2015–2016 El Niño-Southern Oscillation event. *Environ Res Lett* 2018; **13**: 074009.

23. Janssens-Maenhout G, Crippa M and Guizzardi D *et al.* EDGAR v4.3.2 Global Atlas of the three major greenhouse gas emissions for the period 1970–2012. *Earth Syst Sci Data* 2019; **11**: 959–1002.
24. Höglund-Isaksson L. Bottom-up simulations of methane and ethane emissions from global oil and gas systems 1980 to 2012. *Environ Res Lett* 2017; **12**: 024007.
25. Helmig D, Rossabi S and Hueber J *et al.* Reversal of global atmospheric ethane and propane trends largely due to US oil and natural gas production. *Nat Geosci* 2016; **9**: 490–5.
26. Dalsøren SB, Myhre G and Hodnebrog Ø *et al.* Discrepancy between simulated and observed ethane and propane levels explained by underestimated fossil emissions. *Nat Geosci* 2018; **11**: 178–84.
27. Petrenko VV, Smith AM and Schaefer H *et al.* Minimal geological methane emissions during the Younger Dryas–Preboreal abrupt warming event. *Nature* 2017; **548**: 443–6.
28. Hmiel B, Petrenko VV and Dyonisius MN *et al.* Preindustrial ¹⁴CH₄ indicates greater anthropogenic fossil CH₄ emissions. *Nature* 2020; **578**: 409–12.
29. Etiopie G, Ciotoli G and Schwietzke S *et al.* Gridded maps of geological methane emissions and their isotopic signature. *Earth Syst Sci Data* 2019; **11**: 1–22.
30. Naik V, Voulgarakis A and Fiore AM *et al.* Preindustrial to present-day changes in tropospheric hydroxyl radical and methane lifetime from the Atmospheric Chemistry and Climate Model Intercomparison Project (ACCMIP). *Atmos Chem Phys* 2013; **13**: 5277–98.
31. Nicely JM, Canty TP and Manyin M *et al.* Changes in global tropospheric OH expected as a result of climate change over the last several decades. *J Geophys Res Atmos* 2018; **123**: 10774–95.
32. Zhao Y, Saunio M and Bousquet P *et al.* Inter-model comparison of global hydroxyl radical (OH) distributions and their impact on atmospheric methane over the 2000–2016 period. *Atmos Chem Phys* 2019; **19**: 13701–23.
33. Naus S, Montzka SA and Patra PK *et al.* A three-dimensional-model inversion of methyl chloroform to constrain the atmospheric oxidative capacity. *Atmos Chem Phys* 2021; **21**: 4809–24.
34. Patra PK, Krol MC and Prinn RG *et al.* Methyl chloroform continues to constrain the hydroxyl (OH) variability in the troposphere. *J Geophys Res Atmos* 2021; **126**: e2020JD033862.
35. Naus S, Montzka SA and Pandey S *et al.* Constraints and biases in a tropospheric two-box model of OH. *Atmos Chem Phys* 2019; **19**: 407–24.
36. Sherwood OA, Schwietzke S and Arling VA *et al.* Global inventory of gas geochemistry data from fossil fuel, microbial and burning sources, version 2017. *Earth Syst Sci Data* 2017; **9**: 639–56.
37. Feinberg AI, Coulon A and Stenke A *et al.* Isotopic source signatures: impact of regional variability on the $\delta^{13}\text{C}_{\text{CH}_4}$ trend and spatial distribution. *Atmos Environ* 2018; **174**: 99–111.
38. Ganesan AL, Stell AC and Gedney N *et al.* Spatially resolved isotopic source signatures of wetland methane emissions. *Geophys Res Lett* 2018; **45**: 3737–45.
39. Miller SM, Michalak AM and Detmers RG *et al.* China's coal mine methane regulations have not curbed growing emissions. *Nat Commun* 2019; **10**: 303.
40. Poulter B, Bousquet P and Canadell JG *et al.* Global wetland contribution to 2000–2012 atmospheric methane growth rate dynamics. *Environ Res Lett* 2017; **12**: 094013.
41. Bloom AA, Bowman KW and Lee M *et al.* A global wetland methane emissions and uncertainty dataset for atmospheric chemical transport models (WetCHARTs version 1.0). *Geosci Model Dev* 2017; **10**: 2141–56.
42. Taylor KE. Summarizing multiple aspects of model performance in a single diagram. *J Geophys Res Atmos* 2001; **106**: 7183–92.
43. Umezawa T, Brenninkmeijer CAM and Röckmann T *et al.* Interlaboratory comparison of ¹³C and δ ¹³C measurements of atmospheric CH₄ for combined use of data sets from different laboratories. *Atmos Meas Tech* 2018; **11**: 1207–31.
44. Bruhwiler LM, Basu S and Bergamaschi P *et al.* U.S. CH₄ emissions from oil and gas production: have recent large increases been detected? *J Geophys Res Atmos* 2017; **122**: 4070–83.
45. Hristov AN, Harper M and Meinen R *et al.* Discrepancies and uncertainties in bottom-up gridded inventories of livestock methane emissions for the contiguous United States. *Environ Sci Technol* 2017; **51**: 13668–77.
46. Bousquet P, Ciais P and Miller JB *et al.* Contribution of anthropogenic and natural sources to atmospheric methane variability. *Nature* 2006; **443**: 439–43.
47. Andela N, Morton DC and Giglio L *et al.* A human-driven decline in global burned area. *Science* 2017; **356**: 1356–62.
48. Chang J, Peng S and Ciais P *et al.* Revisiting enteric methane emissions from domestic ruminants and their $\delta^{13}\text{C}_{\text{CH}_4}$ source signature. *Nat Commun* 2019; **10**: 3420.
49. McCalley CK, Woodcroft BJ and Hodgkins SB *et al.* Methane dynamics regulated by microbial community response to permafrost thaw. *Nature* 2014; **514**: 478–81.
50. Sweeney C, Dlugokencky E and Miller CE *et al.* No significant increase in long-term CH₄ emissions on North Slope of Alaska despite significant increase in air temperature. *Geophys Res Lett* 2016; **43**: 6604–11.
51. Oh Y, Zhuang Q and Liu L *et al.* Reduced net methane emissions due to microbial methane oxidation in a warmer Arctic. *Nat Clim Chang* 2020; **10**: 317–21.
52. Hopcroft PO, Valdes PJ and O'Connor FM *et al.* Understanding the glacial methane cycle. *Nat Commun* 2017; **8**: 14383.
53. Zhang Z, Zimmermann NE and Stenke A *et al.* Emerging role of wetland methane emissions in driving 21st century climate change. *Proc Natl Acad Sci USA* 2017; **114**: 9647–52.
54. Delwiche KB, Knox SH and Malhotra A *et al.* FLUXNET-CH₄: a global, multi-ecosystem dataset and analysis of methane seasonality from freshwater wetlands. *Earth Syst Sci Data* 2021; **13**: 3607–89.
55. Koffi EN, Bergamaschi P and Alkama R *et al.* An observation-constrained assessment of the climate sensitivity and future trajectories of wetland methane emissions. *Sci Adv* 2020; **6**: eaay4444.
56. Zazzeri G, Lowry D and Fisher RE *et al.* Carbon isotopic signature of coal-derived methane emissions to the atmosphere: from coalification to alteration. *Atmos Chem Phys* 2016; **16**: 13669–80.
57. Vinson DS, Blair NE and Ritter DJ *et al.* Carbon mass balance, isotopic tracers of biogenic methane, and the role of acetate in coal beds: powder river basin (USA). *Chem Geol* 2019; **530**: 119329.
58. Lunt MF, Palmer PI and Lorente A *et al.* Rain-fed pulses of methane from East Africa during 2018–2019 contributed to atmospheric growth rate. *Environ Res Lett* 2021; **16**: 024021.
59. Pandey S, Houweling S and Lorente A *et al.* Using satellite data to identify the methane emission controls of South Sudan's wetlands. *Biogeosciences* 2021; **18**: 557–72.
60. Sapart CJ, Monteil G and Prokopiou M *et al.* Natural and anthropogenic variations in methane sources during the past two millennia. *Nature* 2012; **490**: 85–8.
61. Tans PP. A note on isotopic ratios and the global atmospheric methane budget. *Glob Biogeochem Cycles* 1997; **11**: 77–81.

62. Curry CL. Modeling the soil consumption of atmospheric methane at the global scale: soil consumption of atmospheric methane. *Glob Biogeochem Cycles* 2007; **21**: GB4012.
63. Murguía-Flores F, Arndt S and Ganesan AL *et al*. Soil methanotrophy model (MeMo v1.0): a process-based model to quantify global uptake of atmospheric methane by soil. *Geosci Model Dev* 2018; **11**: 2009–32.
64. Ni X and Groffman PM. Declines in methane uptake in forest soils. *Proc Natl Acad Sci USA* 2018; **115**: 8587–90.
65. Strode SA, Wang JS and Manyin M *et al*. Strong sensitivity of the isotopic composition of methane to the plausible range of tropospheric chlorine. *Atmos Chem Phys* 2020; **20**: 8405–19.
66. Lassey KR, Etheridge DM and Lowe DC *et al*. Centennial evolution of the atmospheric methane budget: what do the carbon isotopes tell us? *Atmos Chem Phys* 2007; **7**: 2119–39.
67. Rice AL, Butenhoff CL and Teama DG *et al*. Atmospheric methane isotopic record favors fossil sources flat in 1980s and 1990s with recent increase. *Proc Natl Acad Sci USA* 2016; **113**: 10791–6.
68. Lassey KR and Ragnauth S. Balancing the global methane budget: constraints imposed by isotopes and anthropogenic emission inventories. *J Integr Environ Sci* 2010; **7**: 97–107.
69. Warwick NJ, Cain ML and Fisher R *et al*. Using $\delta^{13}\text{C}\text{-CH}_4$ and $\delta\text{D}\text{-CH}_4$ to constrain Arctic methane emissions. *Atmos Chem Phys* 2016; **16**: 14891–908.
70. Monteil G, Houweling S and Dlugokenky EJ *et al*. Interpreting methane variations in the past two decades using measurements of CH_4 mixing ratio and isotopic composition. *Atmos Chem Phys* 2011; **11**: 9141–53.
71. Prather MJ, Holmes CD and Hsu J. Reactive greenhouse gas scenarios: systematic exploration of uncertainties and the role of atmospheric chemistry. *Geophys Res Lett* 2012; **39**: L09803.
72. Nicely JM, Salawitch RJ and Canty T *et al*. Quantifying the causes of differences in tropospheric OH within global models: quantifying global model OH differences. *J Geophys Res Atmos* 2017; **122**: 1983–2007.
73. Pandey S, Houweling S and Krol M *et al*. Influence of atmospheric transport on estimates of variability in the global methane burden. *Geophys Res Lett* 2019; **46**: 2302–11.